International Journal for Multidisciplinary Research (IJFMR)
E-ISSN: 2582-2160 ● Website: www.ijfmr.com ● Email: editor@ijfmr.com

DNA-Assisted Assembly of Potassium Iron (III) Oxalate Nanorods

Sameena Yousuf[1], Israel V. M. V. Enoch[2]

[1]Department of Science and Humanities, Nehru Institute of Engineering and Technology, Coimbatore - 641 105, Tamil Nadu, India.
[2]Centre for Nanoscience & Genomics, Karunya Institute of Technology and Sciences (Deemed University), Coimbatore 641114, Tamil Nadu, India.

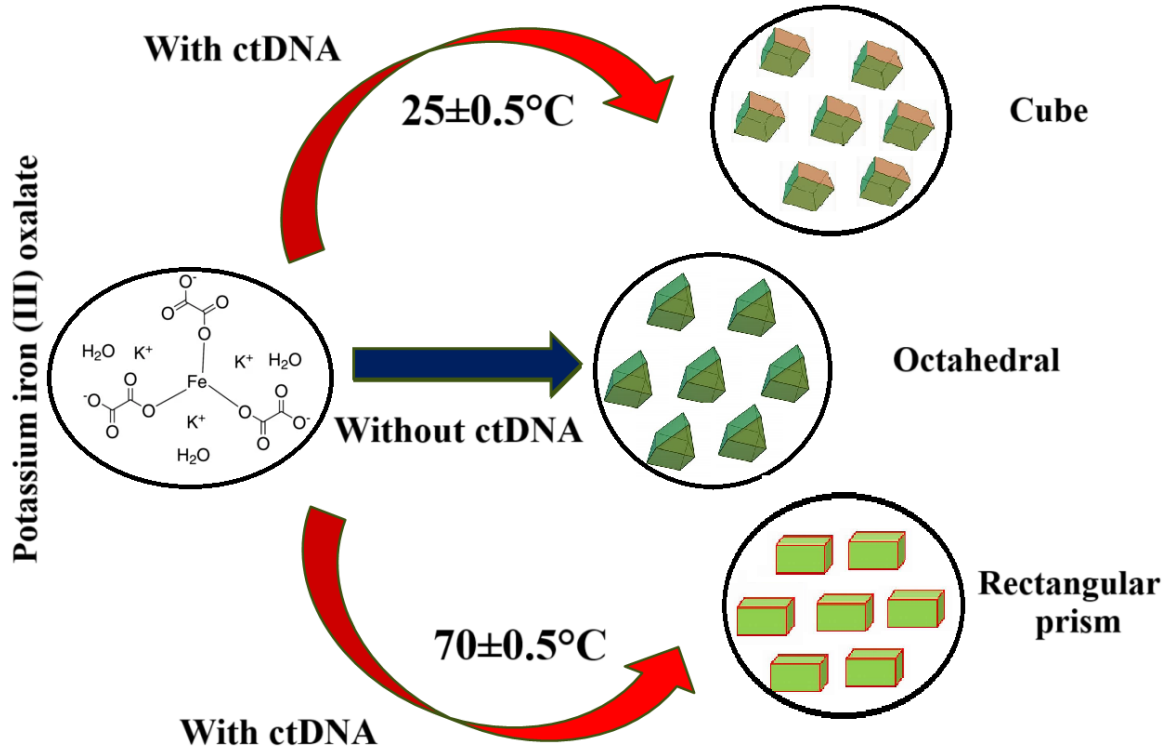

Graphical abstract. Representation of DNA's influence on the assembly of Potassium iron (III) oxalate complex.

ABSTRACT

The present work deals with an assembly of the Potassium iron (III) oxalate complex by calf thymus DNA and the influence of temperature on the DNA-assisted assembly of the metal complex. DNA-assisted assembly of the Potassium iron (III) oxalate complex is studied for its morphological changes at two different temperatures by scanning electron and atomic force microscopy. Calf thymus DNA leads to a 500 nm range cube-shaped Potassium iron (III) oxalate complex at room temperature (25 ± 0.5 °C). On average, 10 µm rectangular prism-shaped nanorods with a diameter of 400 nm complex are observed at higher temperatures (70 ± 0.5°C). The topology of Potassium iron (III) oxalate-calf thymus DNA crystals shows increased surface roughness due to the melting behaviour of ctDNA at the higher temperature. The

templating effect of the DNA on the Potassium iron (III) oxalate complex and its crystallite size is studied by X-ray diffraction analysis. The average crystallite size of calf thymus DNA-assisted Potassium iron (III) oxalate complex at room and high temperatures are 41 and 29 nm respectively. The DNA-assisted assembly can form a long array of Potassium iron (III) oxalate crystals at high temperatures. The morphological behaviour of the complexes with DNA at high temperatures can aid in developing metal complexes with unique therapeutic choices and opportunities.

KEYWORDS: Potassium iron (III) oxalate complex; calf thymus DNA; SEM; AFM; XRD

1. Introduction

DNA is a well-known candidate for molecular and nanomechanical device formulation due to its characteristic molecular recognition, and mechanical properties [1]. In the past decades, the progress of DNA-bound complexes with enhanced functionalities has been reported [2-3]. Although the chemical and photochemical properties of DNA-bound complexes have been extensively studied, inadequate reports to understand the dimensions of the complexes are observed. There is a requirement to find a simple and innovative approach that influences complexes and their dimensions during their DNA binding. This opens new avenues for synthesizing novel complexes with specific sizes and shapes that insight into the fundamental interactions of DNA with the targets. The DNA-bound complexes are interesting substances with potential uses in technology as building blocks for DNA-based novel materials [4]. In this regard, the binding of organic complexes with diverse forms of DNA for their potential medical applications is reported [5]. However, the characteristic chemical, electrochemical, and stereochemical properties of metal complexes and their distinctive responses toward DNA have made them alternative therapeutics to organic molecules in recent years [6, 7]. It is stated that DNA's melting behaviour and denaturation property at high temperatures assist their pairs to open up to assemble fractal metal-based structures. The double strands of DNA get separated into single strands during heating, and endures morphological changes from one form to another form. The work on understanding linear and nonlinear multibranched morphological changes of metal complexes, triggered by DNA denaturation at high temperatures is reported by authors [8]. Considering metal complexes that have been clinically approved for a wide range of medicinal uses, Fe is the most attractive and abundant element present in the environment and participates in various life biochemical processes [9]. The possible multi-dimensional network forms of Fe make it an intriguing building block of complexes [10–12]. Fe in its +3-oxidation state can form an octahedral complex with ligands surrounding the central metal ion. There is an interest in forming metal complexes between Fe and ligands such as oxalate ions due to the flexible bonding style and
choice of the former for the latter. The four oxygen donor atoms of oxalate make a good choice of ligand for building iron oxalate complexes [13]. Among various iron oxalate complexes, the emerald green colour Potassium iron (III) oxalate or known as potassium oxalate ferrate (III) ($[K_3[Fe(C_2O_4)_3]$, KFCO) complex, owns interesting applications in the field of actinometry and photometry, which relate to biomolecular studies and its exploration [14–15]. The paper deals with work of the influence of double-stranded calf thymus DNA (ctDNA) on their assisting behaviour on KFCO's dimension. KFCO is used to grow the crystals of ctDNA-KFCO complex, using ctDNA as an assistant at different temperatures such as room temperature (25 ± 0.5 °C) and higher temperature (70 ± 0.5 °C). The ctDNA-KFCO complex focused on their morphological pattern and their size with the assisting effect of ctDNA in the temperatures studied.

2. Materials and Methods

2.1 Materials

Ferrous ammonium sulphate hexahydrate (99%, Molecular formula $(NH_4)_2Fe(SO_4)_2 \cdot 6H_2O$, Molecular weight 392.14) and oxalic acid (98%, Molecular formula HO_2CCO_2H, Molecular weight 90.03) were procured from Merck (India). ctDNA received from Genei, India was used without further purification. The stock solutions of ctDNA were prepared by dilution of ctDNA as received (1mg/1mL) in 50 mmol NaCl to get 2.27×10^{-4} mol dm^{-3} (per nucleotide phosphate, NP) which was calculated using the molar extinction coefficient of 6600 dm^{-3} mol^{-1} cm^{-1} at 260 nm. The absorbance ratio (A_{260}:A_{280}) in the range of 1.8 to 1.9 is used for the present work. The required concentration of solutions was prepared by dissolving the appropriate amount of it in double distilled water. All other reagents and solvents used were of spectral grade and used as received. The experiments were carried out at an ambient room temperature of 25 ± 0.5 °C and 70 ± 0.5 °C.

2.2 Synthesis of ctDNA-Potassium iron (III) oxalate complex

Scheme 1 represents the synthesis of ctDNA-Potassium iron (III) oxalate complex. Here, 0.5 gm of Ferrous ammonium sulphate hexahydrate dissolved in water (0.2 mol/dm^3 containing 0.1 ml of 3 mol/dm^3 sulphuric acid). 0.3 gm of oxalic acid dissolved in water (0.8 mol/dm^3) was added to the above solution. The obtained yellow precipitate of ferrous oxalate was heated to boiling, allowed to settle and cooled to room temperature. The supernatant solution is decanted and the solid obtained is washed with hot water. The obtained hydrated ferrous oxalate is suspended in a solution of 0.35 gm of Potassium oxalate in water (0.2 mol/dm^3). The above mixture is heated to 40°C followed by the addition of 1 ml H_2O_2 added dropwise with continuous agitation of the mixture. Thus, the obtained greenish liquid filtered from red brown precipitate of iron oxide, is heated to boiling, while the solution of 0.8 gm of oxalic acid added slowly with stirring. The hot liquid filtered and cooled in ice (0 °C). To

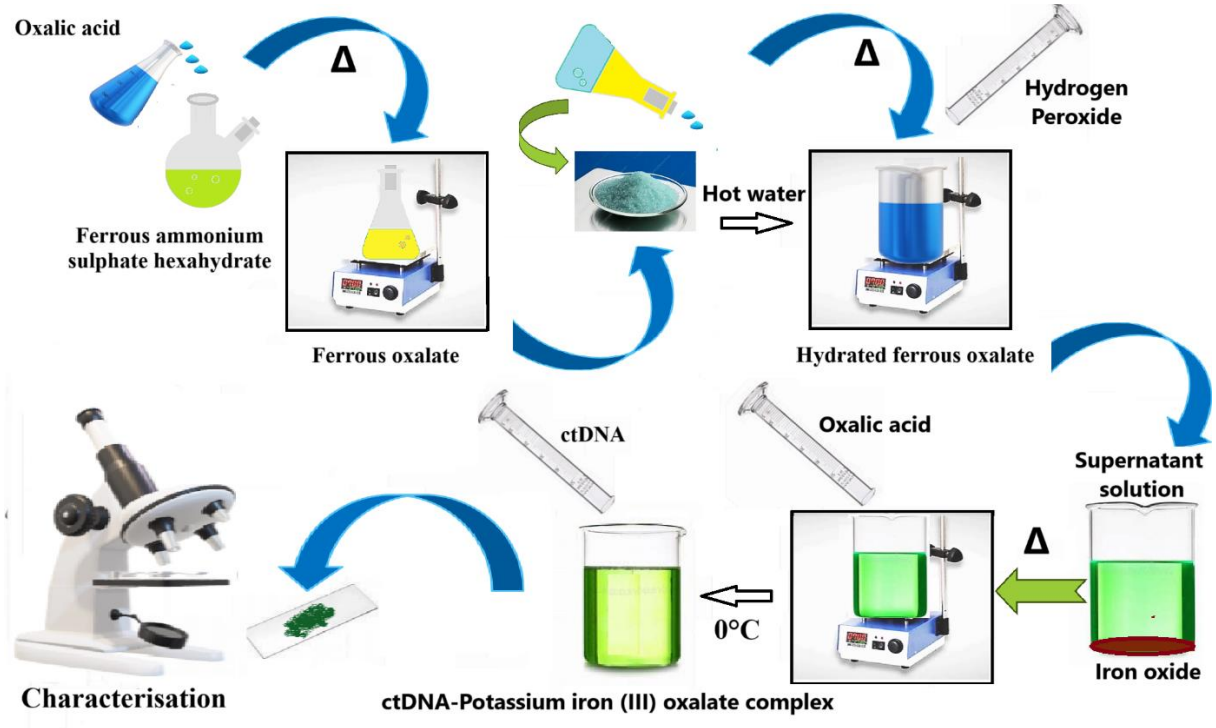

Scheme 1 Representation of ctDNA-Potassium iron (III) oxalate complex synthesis.

the above solution, 2.27 × 10^{-4} mol dm^{-3} ctDNA (1:1) is added and stirred for 30 minutes. Then the spots of the above solution applied on glass plates for spectral, morphological and size characterisation. The ctDNA-Potassium iron (III) oxalate was synthesised at 25 ± 0.5 °C and 70 ± 0.5 °C temperatures. Since DNA plays a significant role in the complex assembly as a function of temperature, a control experiment was carried without the incorporation of DNA, and as a result, the obtained a precipitate of Potassium iron (III) oxalate is studied [16].

2.3 Structural Characterisation

The absorption spectral measurements were carried out with a 1 cm path length cell in UV-Visible spectrophotometer (V-630, Jasco, Japan). Infra-red (IR) spectra were recorded on a Perkin–Elmer spectrometer RXI, USA. The surface topology of the complex is imaged using JEOL JSM 6360 scanning electron microscope (SEM, Japan). The diffraction patterns of the samples were recorded with Shimadzu XRD 6000 X-ray diffractometer (XRD, Japan) using a monochromatic X-ray beam from Cu Kα radiation. The morphology and surface roughness of the complex analysed by Atomic Force Microscope by Nanosurf Easyscan 2.0 instrument (Switzerland) on non-contact mode.

3. Results and discussion

3.1 Binding KFCO with ctDNA

FTIR spectra of ctDNA and its KFCO complex recorded in the liquid state (400-4000 cm^{-1} region) is shown in the Figure 1. The ν(O-H) mode at 3410 cm-1 shows the presence of lattice water molecules in ctDNA and in its KFCO complex. The intensity of this complex was also increased for ctDNA-KFCO interaction. The stretching oxalate modes were completely dominated by the features due to DNA [8, 16]. A new peak emerged at 570 cm^{-1} for the ctDNA-KFCO conjugate, which corresponds to the Fe-O groups, which was not present in the IR spectra of pure ctDNA. Ultra violet–Visible spectra of free ctDNA (4 × 10^{-6} mol dm^{-3}), ctDNA-KFCO complex, (1:1) are shown at different temperatures in Figure 2. UV–visible spectra for both ctDNA and ctDNA-KFCO complex showed the presence of a nucleotide absorbance band at 260 nm, consistent with the spectra for double-stranded DNA. DNA shows the absorption band at 260 nm shifts a ≈2 nm blue shift and there is also an increase in the absorbance of DNA. The evidence for DNA and the complex assembly was obtained by monitoring bands at 260 nm when the suspensions were heated to 70 °C. The increased intensity of the band at 260 nm for ctDNA-KFCO complex at these high temperatures indicated the breaking of double stands into single strands [8]. This band did not show any wavelength shift upon heating, which is consistent with the SEM analysis at different temperatures.

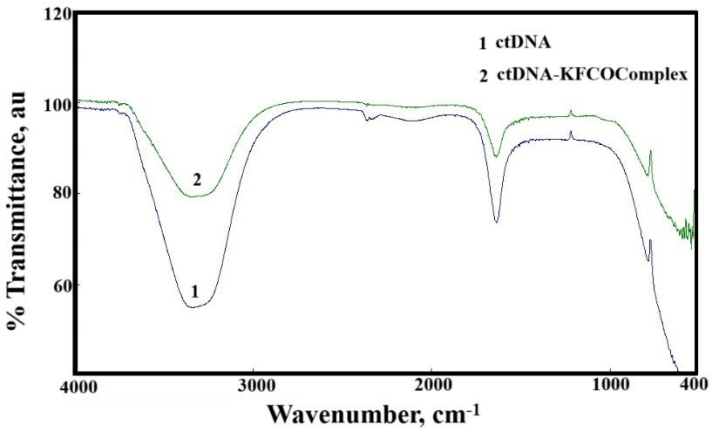

Figure 1. FTIR spectra of ctDNA and its KFCO complex recorded in liquid state.

3.2 Morphological pattern of ctDNA-KFCO complex

The DNA assisted KFCO complex carried at different temperature in solution were spread on a glass substrate and characterized by SEM. Figure 3 shows the SEM image of ctDNA- KFCO complex at room temperature, which showed cube-shaped crystals of KFCO having an average diameter of 500 nm, arranged along the DNA strand framework. The SEM of DNA-KFCO complex carried out at 70 °C is shown in Figure 4. The morphology has changed from a cubic structure to a fractal rectangular prism structure at higher temperature. Each part of the nanorods is about 10 µm in size (Figure 4 inset). The KFCO complex hold their physical shape and size differently at various temperatures. The cube-shaped KFCO crystals are arranged as linear chains, which are joined in the form of a net, guided by DNA strands. On heating at higher temperature, the thermal motion of the molecules results into diffusion of them to form a longer structure. It represents the rectangular prisms structures of ctDNA-KFCO nano rods, with a typical diameter of ~10 µm, formed through aggregation of smaller units into KFCO assemblies of cubic shape, as assisted by ctDNA at high temperature (70 ± 0.5°C). The significant step toward building up of a dendritic architecture by Nickel hexacyanoferrate complex and its control by temperature programming is reported by Bagkar et al. [8].

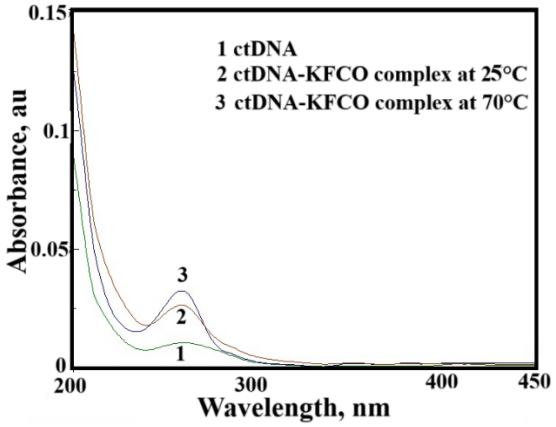

Figure 2. Ultraviolet–Visible spectra of free ctDNA (4×10^{-6} mol dm^{-3}), ctDNA-KFCO complex, (1:1) shown at different temperatures.

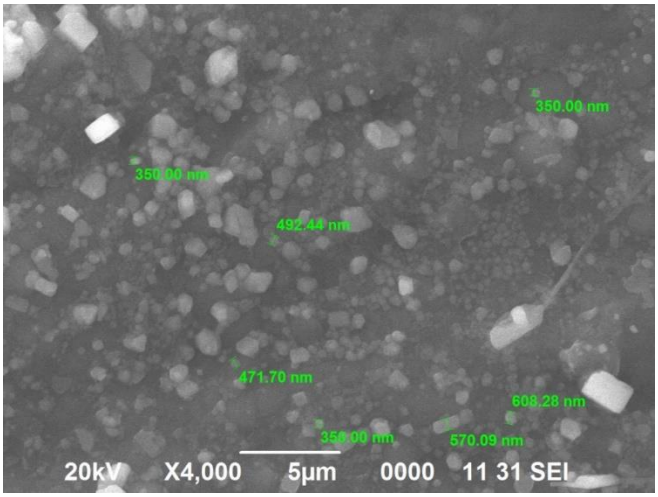

Figure 3. Scanning electron microscopic image of ctDNA- KFCO complex at 25°C temperature.

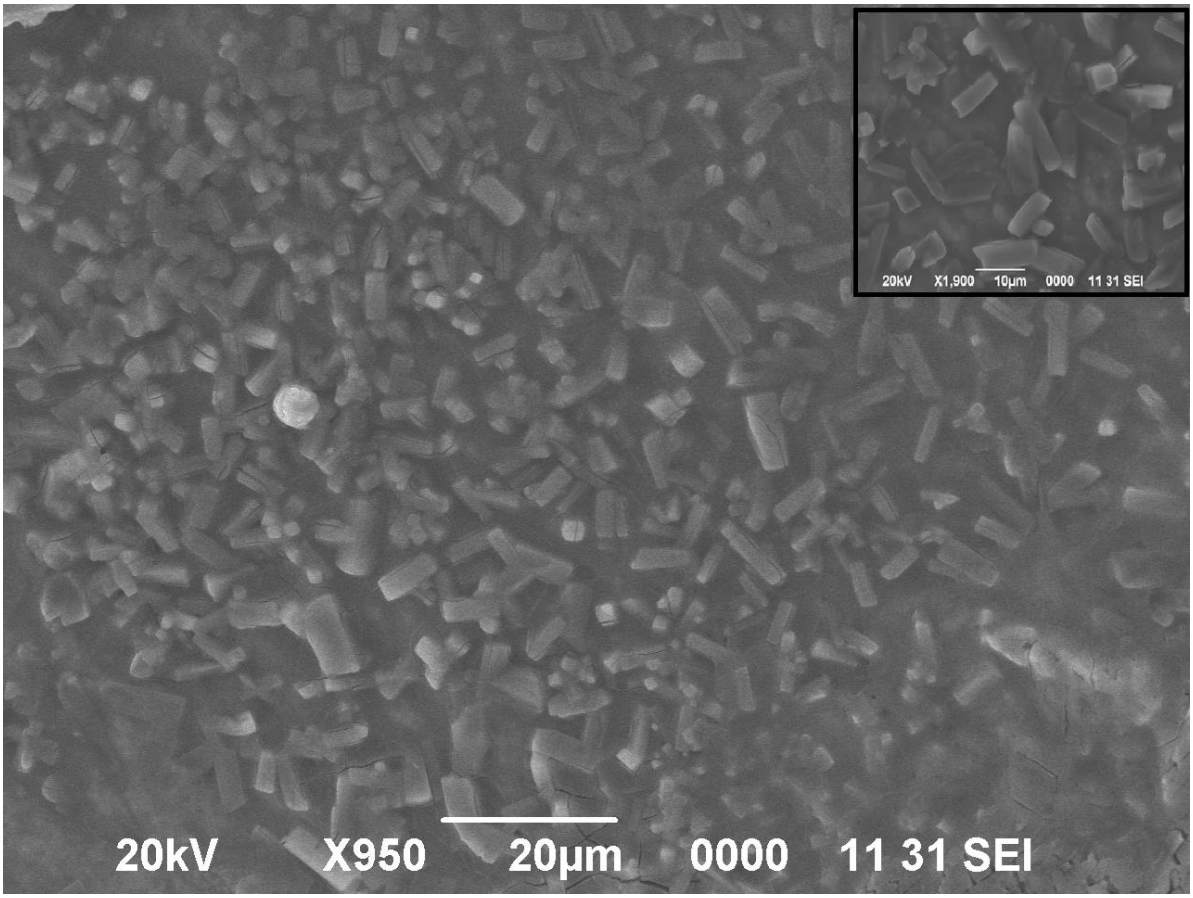

Figure 4. Scanning electron microscopic image of ctDNA-KFCO complex carried out at 70°C.

AFM can provide high-resolution topography data from the angstrom level to the micron scale [17]. The temperature dependence on DNA assisted assembly of KFCO crystals is characterized by AFM (Figure 5 and Figure 6). The 2D image of KFCO complex prepared at room temperature were taken at as positions on the sample. The AFM images obtained for KFCO crystals synthesised at room temperature (Figure 5) reveal a self-aggregation process, mostly in H-type aggregates [18] forming cube shaped geometries of around 140 nm in size. After heating the ctDNA-KFCO complex, the morphology changes and the shape of the particles becomes smaller, around 110 nm in diameter. The H-type aggregation is less pronounced at 70°C and the surface is more evenly covered. The topology of ctDNA-KFCO complex at high temperature shows the rough surface due to denaturation of ctDNA.

3.3 X-ray diffractometric pattern of ctDNA-KFCO complex

The influence of temperature on DNA assisted assembly of KFCO complex in different morphologies, characterized by XRDis shown in Figure 7. It shows the XRD pattern of ctDNA-KFCO complex at room temperature, which showed peak 2θ at 12.1000, 14.5073, 29.1188 degree with variation in its intensity. The ctDNA-KFCO complex at high temperature, form rectangular prisms pattern peak 2θ at 14.5992, 27.1386, and 29.1738 degree. Even though, the distribution of crystals is uniform over a large area, the average crystallite size of the complex prepared at room temperature calculated by Debye Scherrer equation (1) is 41 nm [19].

Crystallite Size, $D = 0.9\lambda/\beta\cos\theta$ (1)

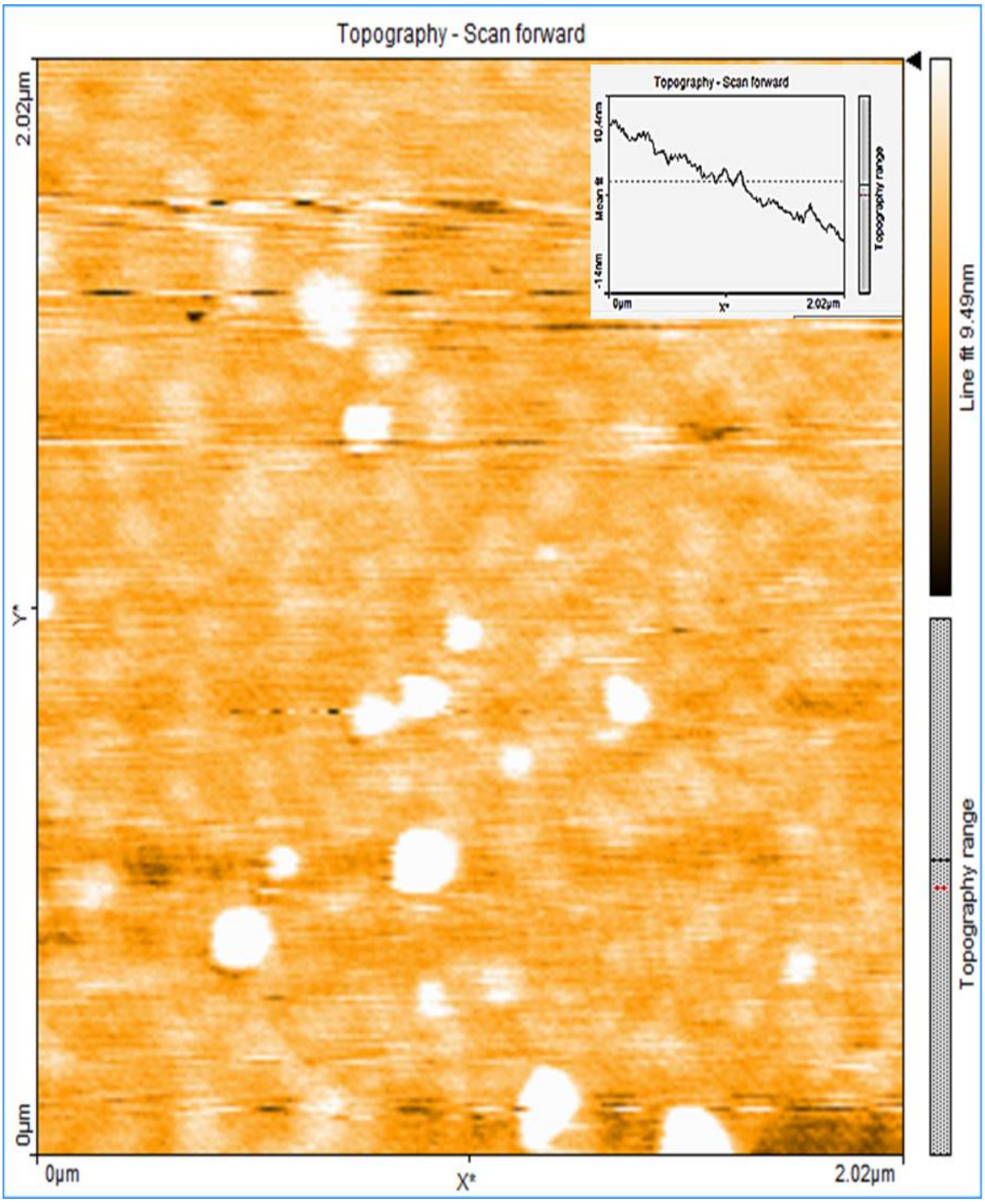

Figure 5. Atomic force microscopic image obtained for KFCO crystals synthesised at 25°C temperature

The crystallite size, D of the complex is calculated by the wavelength of the monochromatic X-ray beam used from Cu Kα radiation (1.5418 Å), the diffraction angle θ, and the broadening factor, FWHM (Fullwidth at half maximum) derived from X-ray diffractogram. The strain (ε) of crystallite size influences the d spacings of the diffractogram. The relation between the ε and peak broadening of the diffractogram produces βε. There is variation of peak broadening occurs due to ε as given in the following equation (2) [19].

$$\text{Peak width, B } (2\theta) = 4\varepsilon \text{Sin}\theta/\text{Cos}\theta \qquad (2)$$

where B and ε represent the peak width and the strain of the complex respectively. The strain of ctDNA-KFCO complex at room and high temperatures are 0.0059 and 0.0064

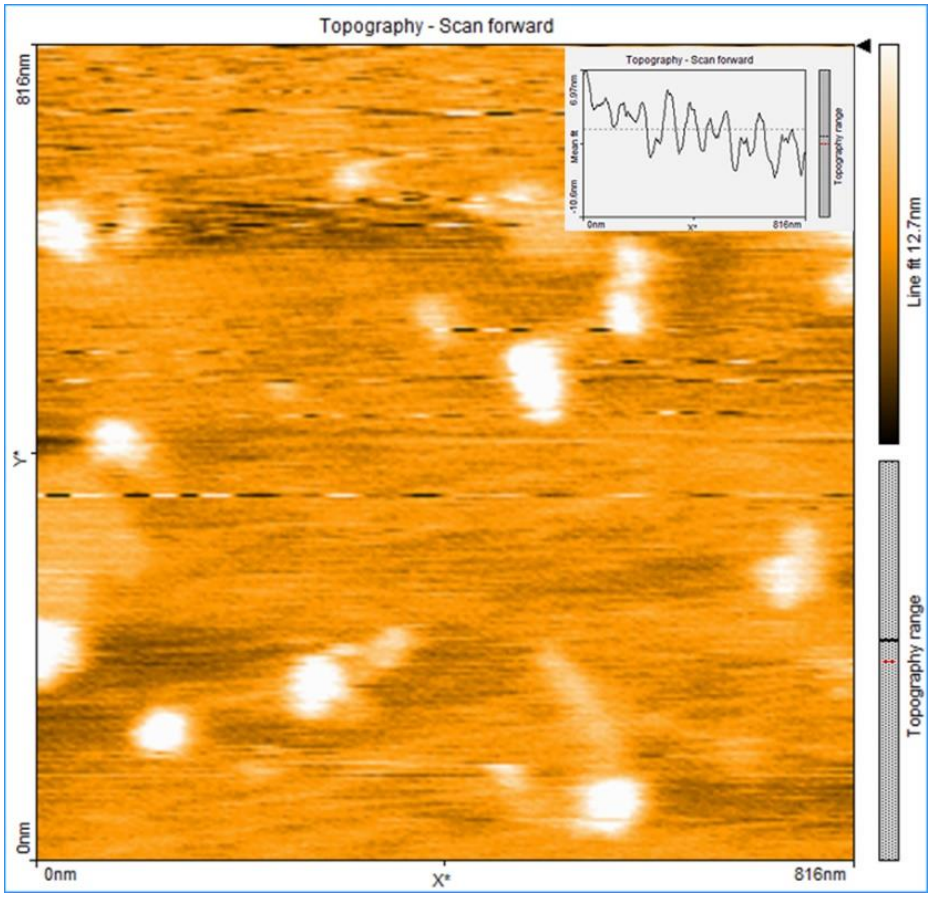

Figure 6. Atomic force microscopic image obtained for KFCO crystals synthesised at 70°C temperature

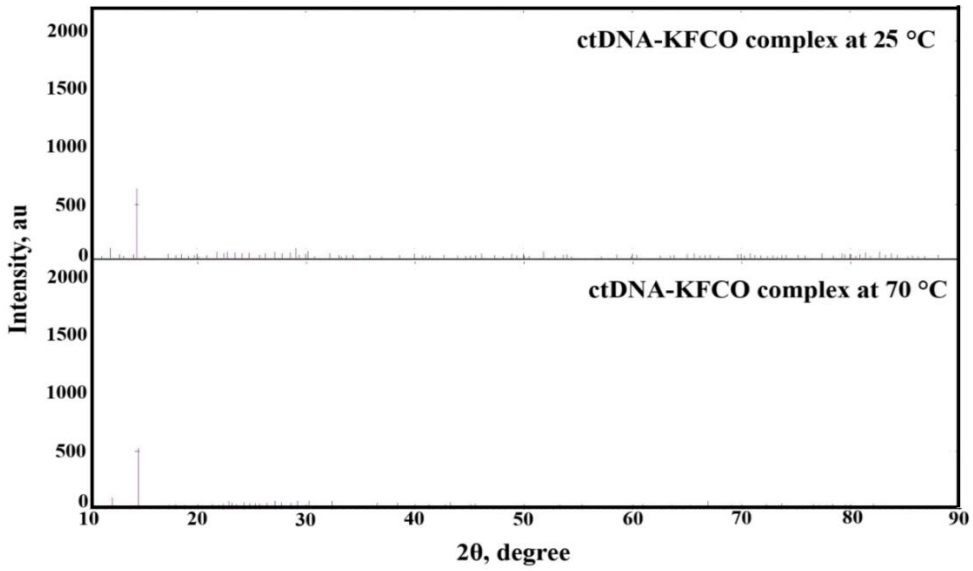

Figure 7. The influence of temperature on DNA-assisted assembly of KFCO complex in different morphologies, characterized by X-ray diffractometry.

respectively. The morphology of ctDNA-KFCO complex has changed from a cubic structure to a fractal rectangular prisms structure. The average crystallite size calculated is 29 nm. It
is found that the lobe of a dendrite is about 10 µm in size. The ctDNA-KFCO complex within these aggregates retain their physical shape and size, as before heating. This indicates the
stabilizing effect that the oligonucleotide has on KFCO complex even at 70°C. The DNA denaturation which starts at about 70 °C, above which the long chain network structure breaks down smaller fragments, subsequent aggregation of which produces nanorods.

4. Conclusion

The double-stranded calf thymus DNA is used as an agent to assemble KFCO complex and to produce aggregates of different morphologies at room and higher temperatures. The study demonstrates a simple method to control the morphologies of calf thymus DNA-KFCO complex by temperature. At 25 °C and 70 °C, DNA assists the assembly, shows cube and rectangular prism shaped arrangement of KFCO complex, leading to the formation of temperature-dependent KFCO complex extended arrays. This DNA-assisted assembly process can be used for the design and fabrication of novel complex architectures of functional nanomaterials.

Funding

This research did not receive any specific grant from funding agencies in the public, commercial, or not-for-profit sectors.

References

1. X. Mao, M. Liu, Q. Li, C. Fan, X. Zuo, DNA-Based Molecular Machines, JACS Au 2, 11 (2022), 2381-2399, DOI: 10.1021/jacsau.2c00292
2. J. Xu, G. A. Wang, L. Gao, et al. Enabling programmable dynamic DNA chemistry using small-molecule DNA binders. Nat. Commun. 14, 4248 (2023). https://doi.org/10.1038/s41467-023-40032-3
3. S. H. F. Abhari, R. D. Felice, Probing electrostatic interactions in DNA-bound CRISPR/Cas9 complexes by molecular dynamics simulations, ACS Omega, DOI: 10.1021/acsomega.4c04359.
4. W. Ma, Y. Zhan, Y. Zhang, et al. The biological applications of DNA nanomaterials: current challenges and future directions. Sig. Transduct. Target. Ther. 6, 351 (2021). https://doi.org/10.1038/s41392-021-00727-9
5. M. Sun, R. Song, Y. Fang, J. Xu, Z. Yang, H. Zhang, ACS Appl. Mater. Interfaces 16 (2024) 51899–51915. DOI: 10.1021/acsami.4c13357
6. J. Karges, R. W. Stokes, S. M. Cohen, Metal complexes for therapeutic applications, Trends in Chem. 3 (2021) 523–534. https://doi.org/10.1016/j.trechm.2021.03.006
7. Rehab H. Elattar, Samah F. El-Malla, Amira H. Kamal, Fotouh R. Mansour, Applications of metal complexes in analytical chemistry: A review article. Coord. Chem. Rev. 501 (2024) 215568. https://doi.org/10.1016/j.ccr.2023.215568.
8. N. Bagkar, S. Choudhury, S. Bhattacharya, J. V. Yakhmi, NA-templated assemblies of nickel hexacyanoferrate crystals. J. Phys. Chem. B 112 (2008) 6467–6472. DOI: 10.1021/jp711536r.
9. M. Ilbert, V. Bonnefoy, Insight into the evolution of the iron oxidation pathways, Biochim. Biophys. Acta - Bioenergetics 1827 (2013) 161–175. https://doi.org/10.1016/j.bbabio.2012.10.001.

10. Y. Gogotsi, Q. Huang, MXenes: Two-Dimensional Building Blocks for Future Materials and Devices, ACS Nano 15 (2021) 5775–5780. DOI: 10.1021/acsnano.1c03161
11. E. C. Theil In: Iron biomineralization. Frankel RB, editor. Plenum Press; 1990
12. P. B. Pansuriya, M. N. Patel, Iron (III) complexes: Preparation, characterization, antibacterial activity and DNA-binding, J. Enzyme Inhibit. Med. Chem. 23 (2008) 230–239. DOI: 10.1080/14756360701474657
13. S. Wafa, J. Abdelhak, A. Arfaoui, H. Amri, K. Boujlel, M. Zid, A. Driss, Oxalate-Bridged Binuclear Iron (III) Complexes of 3, 5-Dimethylpyrazole Ligands: Synthesis, Structure, Spectral and Electrochemical Properties. 31 (2014) 2051–6051.
14. J. Olmsted, Preparation and analysis of potassium tris(oxalato)ferrate (III) trihydrate: A general chemistry experiment. J. Chem. Edu. 61 (1984) 1098. DOI: 10.1021/ed061p1098.
15. L. V. Lutkus, A. Krytenberg, J. Taylor, A. Bhattacharjee, B. A. Steinkamp, T. M. McCormick, Simplification of the potassium ferrioxalate actinometer through carbon dioxide monitoring, Canadian J. Chem. 101 (2022) 171–176, https://doi.org/10.1139/cjc-2022-0188.
16. M. Narsimhulu, K. A. Hussain, IOP Conf. Ser.: Mater. Sci. Eng. 360 (2018) 012048.
17. D. R. Wielgus, B. M. Marzec, A. Zieliński, Characteristics of silver-dopped carbon nanotube coating destined for medical applications, Mater. Today Commun. 38, 2024, 107712, https://doi.org/10.1016/j.mtcomm.2023.107712.
18. H. Yao, K. Domoto, T. Isohashi, K. Kimura, In situ detection of birefringent mesoscopic H and J aggregates of thiacarbocyanine dye in solution, Langmuir 21 (2005) 1067–1073.
19. K. He, N. Chen, C. Wang, L. Wei, J. Chen, Method for determining crystal grain size by X-Ray diffraction. Cryst. Res. Tech. 53 (2018) 1700157.